

Higher-Order Corrections to Quantum Observables in $h \rightarrow WW^*$

Dorival Gonçalves,^a Ajay Kaladharan,^a Alberto Navarro^a

^a*Department of Physics, Oklahoma State University, Stillwater, OK 74078, USA*

E-mail: dorival@okstate.edu, kaladharan.ajay@okstate.edu,
alberto.navarro_serratos@okstate.edu

ABSTRACT: The Higgs boson decay $h \rightarrow WW^* \rightarrow \ell^+ \nu_\ell \ell'^- \bar{\nu}_{\ell'}$ provides a unique window into the structure of the Higgs couplings to electroweak gauge bosons and has recently gained attention for its potential to unveil quantum properties such as quantum entanglement between the intermediate gauge bosons. In this work, we present a systematic study of next-to-leading order electroweak corrections to the angular coefficients characterizing this decay. While these coefficients are highly constrained at leading order, radiative corrections induce shifts of up to 5% to the existing terms and generate novel structures that vanish at leading order, breaking previous relations among coefficients. Despite the impact of these higher-order effects, the $h \rightarrow WW^*$ channel exhibits greater stability under higher-order corrections compared to the previously studied $h \rightarrow ZZ^*$ decay, better preserving the underlying two-qutrit quantum structure.

Contents

1	Introduction	1
2	Quantum Entanglement	2
3	Quantum Tomography	3
4	Analysis	4
4.1	Leading Order Decay	5
4.2	NLO EW Effects	7
4.3	Comparison with the $h \rightarrow e^+e^-\mu^+\mu^-$ Channel	11
5	Summary	12
A	Density Matrix Projection and Entanglement	13

1 Introduction

Precision studies of Higgs boson decays into electroweak gauge bosons, $h \rightarrow ZZ^*, WW^*$, play a central role in the LHC physics program, offering stringent tests of the Standard Model (SM) and sensitive probes of new physics [1–24]. The corresponding angular distributions encode rich information about the nature of the Higgs couplings and potential deviations arising from physics beyond the SM, including novel sources of CP-violation. Recently, it has been proposed that these angular observables can be interpreted through the lens of quantum information theory [25–48]. Within this framework, the reconstruction of the spin density matrix of the diboson system enables the assessment of quantum correlations, most notably entanglement, bringing a compelling new perspective to these studies.¹

In the specific channel $h \rightarrow ZZ^* \rightarrow e^+e^-\mu^+\mu^-$, higher-order corrections have been shown to induce sizable effects, largely shifting the existing leading order (LO) angular coefficients and introducing novel terms comparable in magnitude to the LO contributions [42, 46, 47]. Beyond being crucial for robust new physics searches, these corrections also challenge the two-qutrit interpretation of the system, due to sizable non-factorizable next-to-leading order (NLO) electroweak (EW) contributions [47]. These findings highlight that higher-order effects are not merely a technical refinement, but a qualitative requirement for any consistent quantum information interpretation of the Higgs

¹These quantum observables have also been explored in other LHC processes, most notably in top quark pair production [49–72], where both ATLAS and CMS have recently reported evidence of spin entanglement [73–75]. Furthermore, the possibility that entanglement plays a fundamental role in the emergence of key symmetries in particle physics has also been recently investigated [76–82].

decay $h \rightarrow e^+e^-\mu^+\mu^-$, whether these corrections are incorporated into the signal modeling or considered part of the background [83].

Motivated by these findings, we now turn to the complementary channel $h \rightarrow WW^* \rightarrow \ell^+\nu_\ell\ell'^-\bar{\nu}_{\ell'}$. This mode is of critical importance both experimentally, owing to its large branching fraction, and theoretically, as its angular observables provide independent sensitivity to anomalous Higgs couplings in an effective field theory framework. Unlike the Z boson, which couples to both left- and right-handed fermions, resulting in a moderate spin-analyzing power, the W boson interacts exclusively with left-handed fermions (and right-handed antifermions). This purely chiral structure leads to maximal spin-analyzing power, making the charged leptons in W decays particularly sensitive probes of the boson's polarization and, by extension, of the structure of the Higgs-gauge boson interactions. These distinctive features motivate a dedicated assessment of how NLO EW corrections modify both the angular coefficients² and their implications for the validity of the two-qutrit interpretation in the $h \rightarrow WW^*$ channel.

This paper is organized as follows. In Sec. 2, we review the density matrix formalism and introduce concurrence as a measure of bipartite entanglement. In Sec. 3, we outline the standard quantum tomography framework for reconstructing the WW system at the LHC. In Sec. 4, we present the leading-order and next-to-leading-order electroweak results for the $h \rightarrow WW^* \rightarrow \ell^+\nu_\ell\ell'^-\bar{\nu}_{\ell'}$ process. We derive the angular coefficients, quantify the impact of higher-order effects, and assess their consequences for interpreting the system as a two-qutrit quantum state. A general comparison with the $h \rightarrow e^+e^-\mu^+\mu^-$ channel is also provided. Finally, we summarize our findings and provide an outlook in Sec. 5.

2 Quantum Entanglement

The density matrix ρ plays a central role in quantum mechanics, encapsulating all observable information about a quantum system. For a general mixed state composed of pure states $|\Psi_i\rangle$ with associated classical probabilities p_i , the density matrix can be written as

$$\rho = \sum_i p_i |\Psi_i\rangle\langle\Psi_i|, \quad \text{with } p_i \geq 0, \quad \sum_i p_i = 1. \quad (2.1)$$

A valid physical density matrix must be Hermitian ($\rho^\dagger = \rho$), normalized ($\text{Tr}(\rho) = 1$), and positive semi-definite ($\langle\Psi_i|\rho|\Psi_i\rangle \geq 0$ for all $|\Psi_i\rangle$). In particular, these requirements imply that its eigenvalues λ_i satisfy

$$0 \leq \lambda_i \leq 1, \quad \sum_i \lambda_i = 1. \quad (2.2)$$

Consider now a bipartite system composed of two subsystems, A and B . The full system is said to be separable if its density matrix can be written as a convex sum

$$\rho = \sum_i p_i \rho_A^i \otimes \rho_B^i, \quad \text{with } p_i \geq 0, \quad \sum_i p_i = 1, \quad (2.3)$$

²Angular coefficients are crucial observables for precision studies and searches for physics beyond the SM [42, 46, 47, 84–95]. Hence, it is essential to understand how they are affected by radiative corrections.

where ρ_A^i and ρ_B^i are density matrices acting on the Hilbert spaces of A and B , respectively. If no such decomposition exists, the system is said to be *entangled* [96].

To quantify entanglement, we use the concurrence measure $\mathcal{C}(\rho)$ [97–99], which serves as a well-established indicator of non-separability in bipartite quantum systems. In this study, we consider a system composed of two spin-1 particles, the W bosons originating from the Higgs boson decay, $h \rightarrow WW^*$, forming a two-qutrit quantum system. For generic mixed states, determining $\mathcal{C}(\rho)$ exactly is a nontrivial task, as closed-form expressions are typically limited to two-level (qubit) subsystems. However, the lower and upper bounds on $\mathcal{C}(\rho)$ can be used to estimate entanglement in higher-dimensional settings. These bounds are defined by [30, 100, 101]

$$\begin{aligned} (\mathcal{C}(\rho))^2 &\geq 2 \max \left\{ 0, \text{Tr}[\rho^2] - \text{Tr}[\rho_A^2], \text{Tr}[\rho^2] - \text{Tr}[\rho_B^2] \right\} \equiv \mathcal{C}_{\text{LB}}^2, \\ (\mathcal{C}(\rho))^2 &\leq 2 \min \left\{ 1 - \text{Tr}[\rho_A^2], 1 - \text{Tr}[\rho_B^2] \right\} \equiv \mathcal{C}_{\text{UB}}^2, \end{aligned} \quad (2.4)$$

where $\rho_A = \text{Tr}_B(\rho)$ and $\rho_B = \text{Tr}_A(\rho)$ are the reduced density matrices obtained by partial tracing over the degrees of freedom of the other subsystem. The positive lower bound $\mathcal{C}_{\text{LB}} > 0$ guarantees the presence of entanglement, while the null upper bound $\mathcal{C}_{\text{UB}} = 0$ implies separability. Throughout this work, we use \mathcal{C}_{LB} and \mathcal{C}_{UB} to assess the entanglement properties of the WW^* system in Higgs decays.

3 Quantum Tomography

The WW spin system, as a bipartite state of massive spin-1 particles, is based on a nine-dimensional Hilbert space. To analyze its quantum properties, we parameterize the density matrix using a complete operator basis constructed from irreducible tensor operators. The expansion reads [26, 36]

$$\rho = \frac{1}{9} \left(\mathbb{I}_3 \otimes \mathbb{I}_3 + A_{LM}^1 T_M^L \otimes \mathbb{I}_3 + A_{LM}^2 \mathbb{I}_3 \otimes T_M^L + C_{L_1 M_1 L_2 M_2} T_{M_1}^{L_1} \otimes T_{M_2}^{L_2} \right), \quad (3.1)$$

with implicit summation over the indices $L, L_{1,2} = 1, 2$ and $M, M_{1,2} = -L, \dots, L$. The operators T_M^L form a complete set of normalized irreducible tensors satisfying

$$(T_M^L)^\dagger = (-1)^M T_{-M}^L, \quad \text{Tr} \left[T_M^L (T_M^L)^\dagger \right] = 3. \quad (3.2)$$

We focus on the Higgs decay process $h \rightarrow WW^* \rightarrow \ell^+ \nu_\ell \ell'^- \bar{\nu}_{\ell'}$. Given the mass of the Higgs boson $m_h = 125.09$ GeV [102], one of the W bosons is necessarily off-shell. Nonetheless, it can still be treated as a spin-1 object, as the contribution from the scalar component of its propagator cancels when coupled to massless final-state fermions [26, 103]. For definiteness, we consider the leptonic final state $W^+ \rightarrow e^+ \nu_e$ and $W^- \rightarrow \mu^- \bar{\nu}_\mu$. The decay matrix for the W boson in two leptons reads

$$\Gamma = \frac{1}{4} \begin{pmatrix} 1 + \cos^2 \theta - 2\eta_\ell \cos \theta & \frac{1}{\sqrt{2}} (\sin 2\theta - 2\eta_\ell \sin \theta) e^{i\varphi} & (1 - \cos^2 \theta) e^{i2\varphi} \\ \frac{1}{\sqrt{2}} (\sin 2\theta - 2\eta_\ell \sin \theta) e^{-i\varphi} & 2 \sin^2 \theta & -\frac{1}{\sqrt{2}} (\sin 2\theta + 2\eta_\ell \sin \theta) e^{i\varphi} \\ (1 - \cos^2 \theta) e^{-i2\varphi} & -\frac{1}{\sqrt{2}} (\sin 2\theta + 2\eta_\ell \sin \theta) e^{-i\varphi} & 1 + \cos^2 \theta + 2\eta_\ell \cos \theta \end{pmatrix}, \quad (3.3)$$

where θ and φ are the polar and azimuthal angles of the charged lepton in its parent W boson rest frame. The spin-analyzing power η_ℓ for the decay of a W^- (W^+) boson to a negatively (positively) charged lepton, *i.e.*, a fermion (antifermion), is $\eta_\ell = +1$ (-1), reflecting the purely left-handed structure of the W -lepton interaction. In this study, we adopt the helicity basis to define the lepton angles [26, 104]:

- \hat{z} is the direction of the W^+ boson in the WW rest frame.
- $\hat{x} = \text{sign}(\cos \theta_{\text{CM}})(\hat{p} - \cos \theta_{\text{CM}}\hat{z})/\sin \theta_{\text{CM}}$, where $\hat{p} = (0, 0, 1)$ and $\cos \theta_{\text{CM}} = \hat{p} \cdot \hat{z}$.
- $\hat{y} = \hat{z} \times \hat{x}$.

The normalized differential decay distribution for the process $h \rightarrow WW^* \rightarrow \ell_1^+ \nu_1 \ell_2^- \bar{\nu}_2$ is then expressed as

$$\begin{aligned} \frac{1}{\Gamma} \frac{d\Gamma}{d\Omega_1 d\Omega_2} &= \left(\frac{3}{4\pi}\right)^2 \text{Tr} \left\{ \rho (\Gamma_1 \otimes \Gamma_2)^T \right\} \\ &= \frac{1}{(4\pi)^2} \left[1 + A_{LM}^1 B_L Y_L^M(\theta_1, \varphi_1) + A_{LM}^2 B_L Y_L^M(\theta_2, \varphi_2) \right. \\ &\quad \left. + C_{L_1 M_1 L_2 M_2} B_{L_1} B_{L_2} Y_{L_1}^{M_1}(\theta_1, \varphi_1) Y_{L_2}^{M_2}(\theta_2, \varphi_2) \right], \end{aligned} \quad (3.4)$$

$$(3.5)$$

where $\Gamma_i \equiv \Gamma(\theta_i, \varphi_i)$ for $i = 1, 2$, and $B_1 = -\sqrt{2\pi}\eta_\ell$, $B_2 = \sqrt{2\pi/5}$. The angular coefficients A_{LM}^i and $C_{L_1 M_1 L_2 M_2}$ can be determined from the orthogonality relations of the spherical harmonics:

$$\frac{1}{\sigma} \int \frac{d\sigma}{d\Omega_1 d\Omega_2} Y_L^M(\Omega_i)^* d\Omega_1 d\Omega_2 = \frac{B_L}{4\pi} A_{LM}^i, \quad (3.6)$$

$$\frac{1}{\sigma} \int \frac{d\sigma}{d\Omega_1 d\Omega_2} Y_{L_1}^{M_1}(\Omega_1)^* Y_{L_2}^{M_2}(\Omega_2)^* d\Omega_1 d\Omega_2 = \frac{B_{L_1} B_{L_2}}{(4\pi)^2} C_{L_1 M_1 L_2 M_2}. \quad (3.7)$$

The use of Eq. (3.6) and Eq. (3.7) to extract the angular coefficients guarantees the hermiticity of the spin density matrix ρ , as it leads to the relations $A_{LM}^i = (-1)^M (A_{L, -M}^i)^*$ and $C_{L_1 M_1 L_2 M_2} = (-1)^{M_1 + M_2} (C_{L_1, -M_1, L_2, -M_2})^*$. Moreover, the expansion in Eq. (3.1) enforces the proper normalization of the density matrix. However, the physical requirement that ρ be positive semi-definite is not automatically ensured in this reconstruction [47]. Any violation of this condition typically reflects a breakdown in the modeling assumptions, either in the two-qutrit assumption (3.1), the decay matrix (3.3), or the factorized angular distribution (3.4). We explore the possibility and implications of such breakdowns from NLO EW corrections for the $h \rightarrow WW^*$ decay in Sec. 4.

4 Analysis

The decay channel $h \rightarrow WW^* \rightarrow \ell^+ \nu_\ell \ell'^- \bar{\nu}_{\ell'}$ offers a compelling framework for studying quantum entanglement in a two-qutrit system composed of massive spin-1 gauge bosons at the LHC. A representative sample of Feynman diagrams at leading and next-to-leading electroweak orders is shown in Fig. 1. Due to the scalar nature of the Higgs boson, the

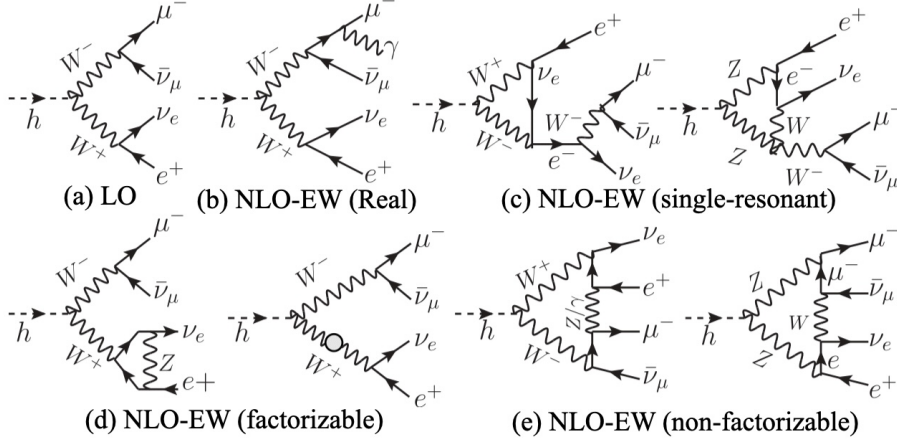


Figure 1. Representative sample of Feynman diagrams for the LO and NLO EW contributions to the Higgs boson decay into four leptons $h \rightarrow e^+ \nu_e \mu^- \bar{\nu}_\mu$.

WW^* system is produced in a spin-correlated state, which, at leading order, enforces strict constraints on the angular coefficients A_{LM}^i and $C_{L_1 M_1 L_2 M_2}$. These symmetries result in a particular texture for the spin density matrix, which implies the presence of quantum entanglement, even for inclusive final-state configurations [25, 26, 30–33, 37–41]. In what follows, we first review the leading-order angular coefficients A_{LM}^i and $C_{L_1 M_1 L_2 M_2}$, and quantify the degree of entanglement for the WW^* system. We then derive how higher-order electroweak corrections modify these observables, and assess their effects on the density matrix and two-qutrit interpretation.

4.1 Leading Order Decay

In the decay $h \rightarrow WW^*$, angular momentum and parity conservation impose strong constraints on the spin correlations, resulting in the following relations among the angular coefficients at LO [26]:

$$\begin{aligned}
 A_{20}^1 &= A_{20}^2 \neq 0, \\
 C_{1,1,1,-1} &= C_{1,-1,1,1} = -C_{2,1,2,-1} = -C_{2,-1,2,1} \neq 0, \\
 C_{2,2,2,-2} &= C_{2,-2,2,2} = -C_{1,0,1,0} = 2 - C_{2,0,2,0} \neq 0, \\
 \frac{A_{20}^{1,2}}{\sqrt{2}} + 1 &= C_{2,2,2,-2}.
 \end{aligned} \tag{4.1}$$

These conditions constrain the LO density matrix to the following form:

$$\rho_{\text{LO}} = \begin{pmatrix} 0 & 0 & 0 & 0 & 0 & 0 & 0 & 0 \\ 0 & 0 & 0 & 0 & 0 & 0 & 0 & 0 \\ 0 & 0 & \frac{1}{3}C_{2,2,2,-2} & 0 & \frac{1}{3}C_{2,1,2,-1} & 0 & \frac{1}{3}C_{2,2,2,-2} & 0 \\ 0 & 0 & 0 & 0 & 0 & 0 & 0 & 0 \\ 0 & 0 & \frac{1}{3}C_{2,1,2,-1} & 0 & \frac{1}{3}(3 - 2C_{2,2,2,-2}) & 0 & \frac{1}{3}C_{2,1,2,-1} & 0 \\ 0 & 0 & 0 & 0 & 0 & 0 & 0 & 0 \\ 0 & 0 & \frac{1}{3}C_{2,2,2,-2} & 0 & \frac{1}{3}C_{2,1,2,-1} & 0 & \frac{1}{3}C_{2,2,2,-2} & 0 \\ 0 & 0 & 0 & 0 & 0 & 0 & 0 & 0 \\ 0 & 0 & 0 & 0 & 0 & 0 & 0 & 0 \end{pmatrix}, \quad (4.2)$$

with only nine nonzero entries, all fully determined by two independent parameters, denoted here as $C_{2,2,2,-2}$ and $C_{2,1,2,-1}$.

To numerically estimate these coefficients and density matrix, we generate events for $h \rightarrow WW^* \rightarrow e^+ \nu_e \mu^- \bar{\nu}_\mu$ at LO with the Prophecy4F package [105]. We adopt the following on-shell input parameters:

$$m_h = 125 \text{ GeV}, \quad \Gamma_h = 4.097 \text{ MeV}, \quad (4.3)$$

$$m_t = 173.2 \text{ GeV}, \quad \Gamma_t = 1.369 \text{ GeV}, \quad (4.4)$$

$$m_W = 80.385 \text{ GeV}, \quad \Gamma_W = 2.085 \text{ GeV}, \quad (4.5)$$

$$m_Z = 91.1876 \text{ GeV}, \quad \Gamma_Z = 2.4952 \text{ GeV}, \quad (4.6)$$

$$G_\mu = 1.1663787 \times 10^{-5} \text{ GeV}^{-2}. \quad (4.7)$$

The EW coupling is fixed with the G_μ scheme and the complex mass scheme is used for the treatment of unstable particles [106, 107]. We then follow the quantum tomography formalism presented in Sec. 3, extracting the angular coefficients using Eq. (3.6) and Eq. (3.7).³ The resulting density matrix reads

$$\rho_{\text{LO}} = \begin{pmatrix} 0 & 0 & 0 & 0 & 0 & 0 & 0 & 0 \\ 0 & 0 & 0 & 0 & 0 & 0 & 0 & 0 \\ 0 & 0 & 0.1972(2) & 0 & -0.3139(3) & 0 & 0.1962(5) & 0 \\ 0 & 0 & 0 & 0 & 0 & 0 & 0 & 0 \\ 0 & 0 & -0.3139(3) & 0 & 0.6037(4) & 0 & -0.3137(3) & 0 \\ 0 & 0 & 0 & 0 & 0 & 0 & 0 & 0 \\ 0 & 0 & 0.1962(5) & 0 & -0.3137(3) & 0 & 0.1968(2) & 0 \\ 0 & 0 & 0 & 0 & 0 & 0 & 0 & 0 \\ 0 & 0 & 0 & 0 & 0 & 0 & 0 & 0 \end{pmatrix}, \quad (4.8)$$

where the zero entries indicate compatibility with zero within numerical uncertainties. A comparison reveals that the structure of the density matrix obtained numerically in Eq. (4.8) is consistent with the analytical form of Eq. (4.2).

³Rather than focusing on the neutrino reconstruction, which can be performed using established methods [108–117], we investigate how the underlying angular coefficients are affected by higher-order corrections. These coefficients form the theoretical benchmark that reconstruction techniques would ultimately aim to approximate.

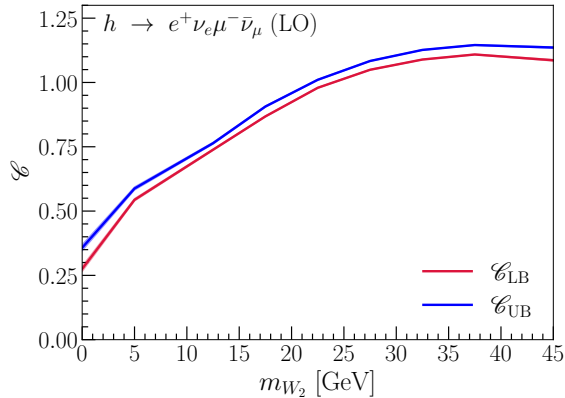


Figure 2. Lower \mathcal{C}_{LB} (red line) and upper \mathcal{C}_{UB} (blue line) bounds of the concurrence for $h \rightarrow WW^* \rightarrow e^+\nu_e\mu^-\bar{\nu}_\mu$ at LO as a function of the off-shell W mass, m_{W_2} .

In Fig. 2, we present the leading order bounds on the concurrence, \mathcal{C}_{LB} and \mathcal{C}_{UB} , as a function of the reconstructed mass of the subleading W boson, m_{W_2} ⁴. The fact that both bounds remain strictly positive across the entire mass range signals the presence of entanglement. Furthermore, the concurrence increases with m_{W_2} , approaching its maximal value as the WW^* system tends toward a pure state [26].

4.2 NLO EW Effects

To evaluate the NLO electroweak (EW) effects, we use `Prophecy4F` with the same input parameters as in the LO analysis, see Eqs. (4.3–4.7), within the complex mass scheme [106, 107, 122]. Photon radiation is included by dressing charged leptons within a cone of $\Delta R(\ell, \gamma) < 0.1$. In Fig. 3, we present the partial decay width for the process $h \rightarrow e^+\nu_e\mu^-\bar{\nu}_\mu$ at LO and NLO EW, along with the corresponding NLO/LO ratio, shown as a function of the highest and lowest reconstructed invariant masses of the $\ell\nu_\ell$ pairs, denoted as m_{W_1} and m_{W_2} , respectively. We assume perfect reconstruction of the neutrino momenta, focusing on the higher-order effects. The distributions reveal that the dominant contribution to the partial Higgs decay width arises when the leading mass is

⁴We used the publicly available Python package `pyerrors` [118], which is based on the Γ -method [119–121] to propagate the uncertainties from the density matrix to its eigenvalues and concurrence bounds.

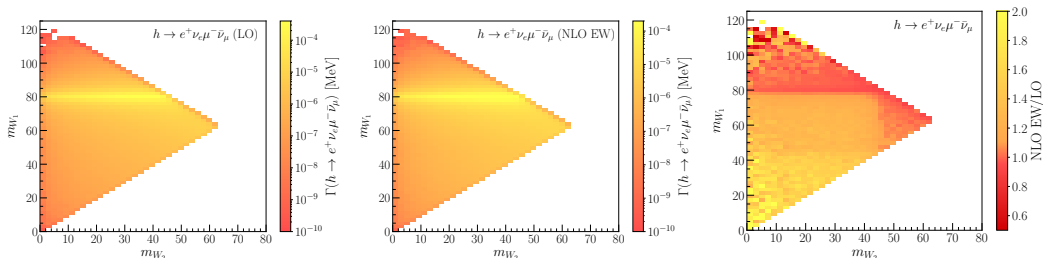


Figure 3. Decay distribution for $h \rightarrow e^+\nu_e\mu^-\bar{\nu}_\mu$ at LO (left panel), NLO EW (central panel), and their corresponding NLO/LO ratios (right panel) in the m_{W_1} - m_{W_2} plane.

Coefficient	LO	NLO EW	NLO/LO
$A_{2,0}^1$	-0.5769(6)	-0.550(1)	0.953
$A_{2,0}^2$	-0.5763(6)	-0.550(1)	0.954
$C_{1,0,1,0}$	-0.5917(3)	-0.6034(4)	1.0198
$C_{1,1,1,-1}$	0.9439(3)	0.9429(3)	0.9989
$C_{2,1,2,-1}$	-0.939(1)	-0.949(2)	0.989
$C_{2,0,2,0}$	1.401(2)	1.383(2)	0.987
$C_{2,2,2,-2}$	0.5885(5)	0.590(1)	1.002
$A_{1,0}^1$	0	-0.0122(3)	-
$A_{1,0}^2$	0	-0.0115(3)	-
$C_{1,-1,2,1}$	0	-0.0153(6)	-
$C_{1,0,2,0}$	0	0.0244(7)	-
$C_{2,-1,1,1}$	0	-0.0169(6)	-
$C_{2,0,1,0}$	0	0.0232(7)	-

Table I. The non-vanishing coefficients for the $h \rightarrow e^+ \nu_e \mu^- \bar{\nu}_\mu$ decay at LO, NLO EW, and their NLO/LO ratio. The index $i = 1, 2$, as used for example in A_{LM}^i , denotes the polarization of W^+ and W^- bosons, respectively. Additional non-vanishing $C_{L_1 M_1 L_2 M_2}$ coefficients can be obtained from those shown using the relation $C_{L_1 M_1 L_2 M_2} = (-1)^{M_1 + M_2} (C_{L_1, -M_1, L_2, -M_2})^*$, which follows from the symmetry properties of spherical harmonics. Charged leptons are dressed with photons using a recombination radius of $\Delta R(\ell, \gamma) < 0.1$.

near the W pole, $|m_{W_1} - m_W| \lesssim 10$ GeV, while the subleading mass lies in the range $10 \text{ GeV} \lesssim m_{W_2} \lesssim 40$ GeV. In this region, the NLO/LO ratio remains close to unity, indicating mild higher-order corrections. This moderate behavior is also reflected in the integrated NLO EW correction to the partial width, with $\delta\Gamma_{\text{NLO}}/\Gamma_{\text{LO}} \simeq 1\%$.

We now investigate the impact of higher-order corrections on the angular coefficients. In [Tab. I](#), we present the non-vanishing coefficients, within uncertainties, for the decay $h \rightarrow e^+ \nu_e \mu^- \bar{\nu}_\mu$ at LO, NLO EW, and their corresponding NLO/LO ratio. Systematic uncertainties due to the missing two-loop EW contribution are estimated by taking the square of the known one-loop corrections [123]. The uncertainties shown in parentheses account for both statistical and systematic errors propagated from the angular distributions. We observe that the LO relations given by [Eq. \(4.1\)](#) are visibly violated at NLO. This is reflected in corrections of up to $\sim 5\%$ to previously dominant coefficients, as well as the emergence of novel angular coefficients that vanish at LO, enriching the angular dynamics.

Angular observables provide sensitive probes of physics beyond the Standard Model. To draw robust conclusions, it is crucial to evaluate these observables with high precision, including higher-order corrections. However, the interpretation of the process as a two-qutrit system, and consequently the applicability of the quantum tomography framework described in [Sec. 3](#), becomes questionable once NLO electroweak corrections are considered. Several types of radiative corrections challenge this interpretation. For instance, virtual contributions, such as the single-resonant topology illustrated in [Fig. 1 \(c\)](#) and the non-factorizable diagrams in [Fig. 1 \(e\)](#), indicate that the two-qutrit system defined

in Eq. (3.1) and the factorized form of the cross section in Eq. (3.4) may no longer hold. Moreover, the presence of real photon emission, depicted in Fig. 1 (b), when the photon is not recombined, alters the form of the decay matrix from Eq. (3.3). These radiative effects call into question the applicability of the idealized tomography formalism in Sec. 3, suggesting that the interpretation of the WW^* system as a two-qutrit quantum state may break down once full NLO corrections are taken into account.

To assess the numerical impact of higher-order effects on the validity of the two-qutrit interpretation, we apply the quantum tomography procedure described in Sec. 3 and examine whether the fundamental properties of the reconstructed density matrix are preserved. The resulting matrix, including full NLO electroweak corrections, takes the form

$$\rho_{\text{NLO}} = \begin{pmatrix} 0.0023(2) & 0 & 0 & 0 & 0 & 0 & 0 & 0 & 0 \\ 0 & -0.0056(3) & 0 & 0.0065(3) & 0 & 0 & 0 & 0 & 0 \\ 0 & 0 & 0.2021(2) & 0 & -0.3152(3) & 0 & 0.1966(5) & 0.0011(3) & 0 \\ 0 & 0.0065(3) & 0 & -0.0054(3) & 0 & 0 & 0 & 0 & 0 \\ 0 & 0 & -0.3152(3) & 0 & 0.5913(5) & 0 & -0.3157(3) & 0 & 0 \\ 0 & 0 & 0 & 0 & 0 & 0.0066(3) & 0 & -0.0042(3) & 0 \\ 0 & 0 & 0.1966(5) & 0 & -0.3157(3) & 0 & 0.2021(2) & 0 & 0 \\ 0 & 0 & 0.0011(3) & 0 & 0 & -0.0042(3) & 0 & 0.0070(3) & 0 \\ 0 & 0 & 0 & 0 & 0 & 0 & 0 & 0 & 0 \end{pmatrix}, \quad (4.9)$$

where the vanishing entries are consistent with zero within 1σ uncertainties. Compared to the LO case shown in Eqs. (4.2) and (4.8), the NLO corrections introduce both modifications to existing angular coefficients and entirely new nonzero components, resulting in a new texture for the density matrix at NLO. As remarked in Sec. 3, the presented quantum tomography enforces hermiticity and normalization of the density matrix. However, it does not automatically guarantee that the matrix is positive semi-definite, a critical physical requirement. To test this condition, we evaluate the eigenvalues of ρ_{NLO} and find that the smallest eigenvalue is negative, $-0.0122(5)$, with another negative eigenvalue of significantly smaller magnitude, $-0.0007(3)$. These results formally signal the breakdown of the two-qutrit interpretation due to higher-order effects.

While the negative eigenvalues are already very small, we investigate strategies to further suppress the undesired contributions and potentially restore a more robust two-qutrit description of the $h \rightarrow e^+ \nu_e \mu^- \bar{\nu}_\mu$ decay at NLO. In Fig. 4 (left panel), we present the lowest eigenvalue of the NLO density matrix as a function of the two-dimensional distribution (m_{W_2}, m_{W_1}) . Whereas the smallest eigenvalue takes on negative values across the phase space, it approaches zero when the leading reconstructed mass, m_{W_1} , lies close to the W boson pole. This kinematic configuration suppresses the non-factorizable contributions, such as those illustrated in Fig. 1 (e), thus improving the validity of the two-qutrit description. Fortunately, this can be achieved with minimal impact on the number of events, as this kinematic regime displays the bulk of the $h \rightarrow e^+ \nu_e \mu^- \bar{\nu}_\mu$ events, as shown in Fig. 3. For more details on the angular coefficients in the scenario where m_{W_1} is selected close to the W boson pole, $|m_{W_1} - m_W| < 10$ GeV, see Tab. II. Another relevant kinematic handle is the dependence on the invariant mass m_{W_2} . The central and right

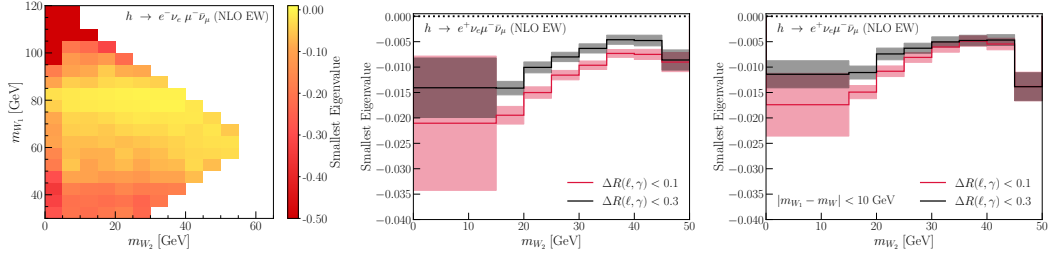


Figure 4. Smallest eigenvalue of the density matrix ρ_{NLO} as a function of the two-dimensional distribution (m_{W_2}, m_{W_1}) . The central panel shows the same quantity as a function of m_{W_2} and the right panel displays it after imposing a cut on the reconstructed mass closest to the W boson pole, $|m_{W_1} - m_W| < 10$ GeV. The left panel assumes the photon-lepton recombination criterion $\Delta R(\ell, \gamma) < 0.1$, whereas the central and right panels display results for two possible criteria: $\Delta R(\ell, \gamma) < 0.1$ (red) and $\Delta R(\ell, \gamma) < 0.3$ (black).

Coefficient	LO	NLO EW	NLO/LO
$A_{2,0}^1$	-0.5284(6)	-0.5120(6)	0.9689
$A_{2,0}^2$	-0.5276(6)	-0.5122(6)	0.9708
$C_{1,0,1,0}$	-0.6261(4)	-0.6350(5)	1.0142
$C_{1,1,1,-1}$	0.9777(4)	0.9790(2)	1.0013
$C_{2,1,2,-1}$	-0.973(1)	-0.983(2)	1.010
$C_{2,0,2,0}$	1.367(2)	1.359(2)	0.994
$C_{2,2,2,-2}$	0.623(2)	0.629(2)	1.009
$A_{1,0}^1$	0	-0.0074(3)	—
$A_{1,0}^2$	0	-0.0067(3)	—
$C_{1,-1,2,1}$	0	-0.0105(7)	—
$C_{1,0,2,0}$	0	0.0138(9)	—
$C_{2,-1,1,1}$	0	-0.0117(8)	—
$C_{2,0,1,0}$	0	0.0129(9)	—
$C_{1,-1,1,0}$	0	0.0010(3)	—
$C_{2,-2,2,1}$	0	0.005(1)	—

Table II. The non-vanishing coefficients for the $h \rightarrow e^+ \nu_e \mu^- \bar{\nu}_\mu$ decay at LO, NLO EW, and their NLO/LO ratio. The invariant mass conditions $|m_{W_1} - m_W| < 10$ GeV and $m_{W_2} > 10$ GeV are imposed. Charged leptons are dressed with photons using a recombination radius of $\Delta R(\ell, \gamma) < 0.1$.

panels of Fig. 4 show a pronounced dependence of the lowest eigenvalue with m_{W_2} , reaching values of order $\mathcal{O}(10^{-3})$ in the range $30 \text{ GeV} \lesssim m_{W_2} \lesssim 45 \text{ GeV}$. Further improvements can be achieved by increasing the radius in the photon-lepton recombination criterion, as illustrated in Fig. 4 (central and right panels), where the recombination radius is varied from $\Delta R(\ell, \gamma) < 0.1$ to 0.3. A larger recombination radius mitigates the impact of events in which the photon does not cluster with its parent lepton, events that are not accurately described by the decay matrix in Eq. (3.3).

While negative eigenvalues are formally present, their numerical impact is subleading.

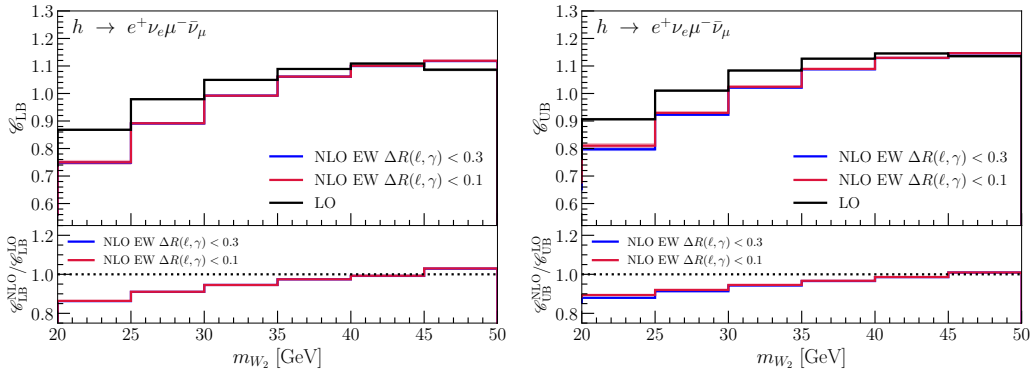


Figure 5. Lower \mathcal{C}_{LB} (left panel) and upper \mathcal{C}_{UB} (right panel) bounds of the concurrence for $h \rightarrow WW^* \rightarrow e^+\nu_e\mu^-\bar{\nu}_\mu$ as a function of the off-shell W mass, m_{W_2} . The results are presented at LO (black) and NLO EW with recombination radius $\Delta R(\ell, \gamma) < 0.1$ (red) and $\Delta R(\ell, \gamma) < 0.3$ (blue).

Hence, the fundamental properties of the two-qutrit density matrix remain satisfied to a very good approximation at NLO EW, justifying the evaluation of the entanglement measure of the two-qutrit system at this level of precision. In Fig. 5, we present the lower and upper bounds of the concurrence at LO and NLO EW.⁵ For consistency, we restrict the analysis to the region where negative eigenvalues remain below $\mathcal{O}(10^{-2})$, which corresponds to $m_{W_2} \gtrsim 20$ GeV. We find that higher-order corrections yield a qualitatively similar entanglement pattern to the LO prediction, with a moderate degradation of at most 10% at low m_{W_2} , and a closer agreement with the LO behavior at higher values of m_{W_2} . We perform the NLO EW analysis for two photon-lepton recombination scenarios: $\Delta R(\ell, \gamma) < 0.1$ (red line) and $\Delta R(\ell, \gamma) < 0.3$ (blue line). The differences between these choices in the lower and upper bounds of the entanglement measure are found to be subleading.

4.3 Comparison with the $h \rightarrow e^+e^-\mu^+\mu^-$ Channel

It is instructive to compare the present analysis of NLO electroweak effects to angular coefficients in the $h \rightarrow WW^* \rightarrow e^+\nu_e\mu^-\bar{\nu}_\mu$ channel with the corresponding study of the $h \rightarrow ZZ^* \rightarrow e^+e^-\mu^+\mu^-$ decay [42, 46, 47]. In the $h \rightarrow e^+\nu_e\mu^-\bar{\nu}_\mu$ channel, the absence of electric charge on neutrinos eliminates entire classes of photon-exchange loop topologies, such as those connecting neutrino lines or neutrinos to charged leptons, and also suppresses final-state photon radiation. Furthermore, the fixed helicity correlation between charged leptons and neutrinos from W decay constrains interference with loop diagrams, since helicity flips require mass-suppressed terms. These factors strongly reduce loop-induced angular structures. Conversely, the $h \rightarrow e^+e^-\mu^+\mu^-$ channel involves only charged leptons, allowing photons to connect any pair of external legs. Moreover, the presence of both left-

⁵Since the negative eigenvalues are comparatively small in magnitude, we neglect their existence when evaluating the concurrence bounds. The validity of this approximation is examined in App. A, where we compare these results with those obtained from the projected density matrix, defined as the closest positive semi-definite Hermitian matrix with unit trace. The distance between the matrices is defined by the Frobenius norm [124].

and right-handed couplings at LO leads to a rich interference pattern at NLO, generating nontrivial loop-induced structures that significantly modify angular coefficients.

These general expectations are confirmed numerically. In the four-charged-lepton final state, the NLO EW corrections induce significantly more pronounced effects to the angular coefficients, both by substantially shifting the existing LO terms and by introducing new coefficients that vanish at LO but appear at NLO with magnitudes comparable to the leading ones. In particular, these effects substantially impact the texture of the density matrix, as evidenced by the comparison between the LO and NLO results presented in Eqs. (4.7) and (4.8) of Ref. [47] (see also Table VI in the same reference). As a result, the smallest eigenvalue of the density matrix in that case remained negative, reaching values as low as ~ -0.2 even under optimal kinematic selections, challenging the two-qudit interpretation of the system [47]. In contrast, the current $h \rightarrow e^+ \nu_e \mu^- \bar{\nu}_\mu$ analysis reveals only moderate NLO effects to the angular coefficients, resulting in milder distortions in the density matrix structure. The resulting negative eigenvalues are suppressed by approximately two orders of magnitude with respect to the four charged lepton channel, see Fig. 4, indicating a significantly better preservation of the two-qudit structure and showing that this channel is more robust against non-factorizable contributions from higher-orders. For more details on the consistency of the density matrix in both channels, see App. A.

5 Summary

The Higgs boson decay $h \rightarrow WW^* \rightarrow \ell^+ \nu_\ell \ell'^- \bar{\nu}_{\ell'}$ provides a unique window into the structure of Higgs boson couplings to electroweak gauge bosons. These interactions manifest in the angular distributions of the final-state leptons, making the associated angular coefficients from gauge boson decays powerful observables for testing SM predictions and uncovering potential signs of new physics. More recently, a novel and complementary perspective has emerged by interpreting these coefficients through the framework of quantum information theory, such as by assessing whether the gauge bosons exhibit quantum entanglement, enriching the phenomenological relevance of such observables.

In this work, we have presented a systematic study of higher-order electroweak corrections to the angular coefficients in the $h \rightarrow WW^* \rightarrow \ell^+ \nu_\ell \ell'^- \bar{\nu}_{\ell'}$ channel. At leading order, the angular coefficients for the $h \rightarrow \ell^+ \nu_\ell \ell'^- \bar{\nu}_{\ell'}$ system are highly constrained by the spin and parity of the Higgs boson, yielding a density matrix with only nine non-vanishing entries, governed by just two independent parameters. This compact structure leads to a physically consistent, entangled two-qudit quantum system, even when no phase-space cuts are applied. When NLO electroweak corrections are included, this structure is deformed. New angular coefficients acquire nonzero values and the previous relations among angular coefficients are broken. These deviations arise from various radiative effects, including singly-resonant topologies, non-factorizable contributions, and real photon emissions in the final state.

A particularly illuminating comparison can be drawn between the present analysis of NLO electroweak corrections to angular coefficients in $h \rightarrow WW^* \rightarrow e^+ \nu_e \mu^- \bar{\nu}_\mu$ and the

corresponding study of $h \rightarrow ZZ^* \rightarrow e^+e^-\mu^+\mu^-$ presented in Ref. [47]. We find that the angular coefficients in the $h \rightarrow e^+\nu_e\mu^-\bar{\nu}_\mu$ decay exhibit greater resilience to radiative effects than the $h \rightarrow e^+e^-\mu^+\mu^-$ counterpart. In the latter, NLO EW corrections, especially those arising from singly-resonant topologies, significantly distort the angular coefficients and undermine the validity of the two-qutrit interpretation. In contrast, the $h \rightarrow WW^*$ channel displays milder corrections, better preserving the two-qutrit system.

In conclusion, our results highlight the importance of accounting for higher-order electroweak effects when studying quantum observables at colliders. While leading-order analyses offer valuable theoretical guidance, they may fail to capture the full quantum structure of realistic events. Incorporating radiative corrections is essential not only for achieving precision in Higgs coupling measurements, but also for enabling a robust interpretation of emergent quantum features, such as quantum entanglement, in collider experiments.

Acknowledgments

We thank Frank Krauss for his previous collaboration and valuable discussions. We are also grateful to Ansgar Denner and Stefan Dittmaier for clarifications regarding Prophecy4f. The work of DG, AK, and AN is supported in part by US Department of Energy Grant Number DE-SC 0016013. Some computing for this project was performed at the High Performance Computing Center at Oklahoma State University, supported in part through the National Science Foundation grant OAC-1531128.

A Density Matrix Projection and Entanglement

Since the reconstructed density matrix for $h \rightarrow e^+\nu_e\mu^-\bar{\nu}_\mu$ decay at NLO EW exhibits small negative eigenvalues, we project this density matrix, ρ , onto the nearest positive semi-definite Hermitian matrix with unit trace, ρ^{proj} . The distance between matrices is quantified using the Frobenius norm [124]

$$|\rho^{\text{proj}} - \rho|_F \equiv \sqrt{\sum_{i,j} |\rho_{ij}^{\text{proj}} - \rho_{ij}|^2}. \quad (\text{A.1})$$

We employ the Python package QuTiP [125, 126] to obtain the projected density matrix that minimizes the Frobenius norm.

To assess the validity of neglecting the small negative eigenvalues, we compare the concurrence bounds obtained using the original density matrix ρ and the projected matrix ρ^{proj} in Fig. 6 (top panel). The lower panel of each plot shows the Frobenius norm $|\rho^{\text{proj}} - \rho|_F$ between the two matrices. In this analysis, we consider only the central value of ρ and neglect its uncertainties. We find that the concurrence bounds are nearly identical in both cases. Notably, the difference in \mathcal{C}_{LB} is only about 0.2% in the bin $35 \text{ GeV} < m_{W_2} < 45 \text{ GeV}$, where the magnitude of the smallest negative eigenvalue is greatly suppressed to ~ -0.005 . A more noticeable difference of about 4% in \mathcal{C}_{LB} appears

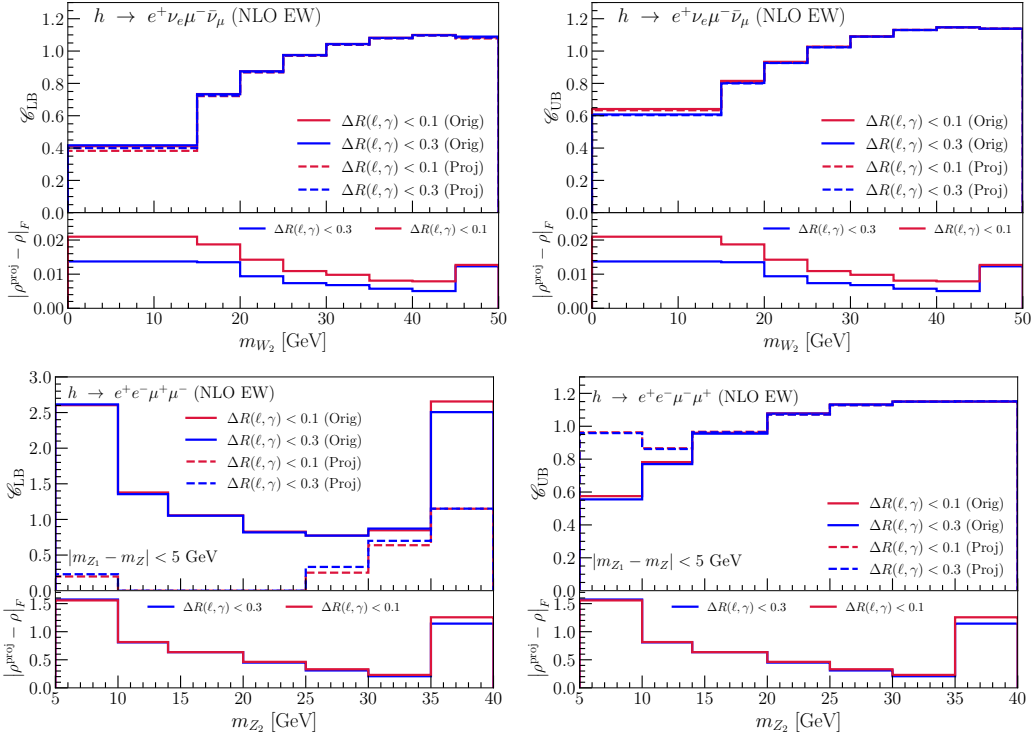


Figure 6. Lower \mathcal{C}_{LB} (left panel) and upper \mathcal{C}_{UB} (right panel) bounds of the concurrence for $h \rightarrow e^+ \nu_e \mu^- \bar{\nu}_\mu$ (top) and $h \rightarrow e^+ e^- \mu^+ \mu^-$ (bottom) as a function of the off-shell W mass, m_{W_2} . The results are presented at NLO EW with recombination radii $\Delta R(\ell, \gamma) < 0.1$ (red) and $\Delta R(\ell, \gamma) < 0.3$ (blue). Concurrence bounds computed from the original density matrix ρ are shown as solid lines, while those from the projected matrix ρ^{proj} appear as dashed lines. We also present the Frobenius norm between the two matrices, $|\rho^{\text{proj}} - \rho|_F$, in the bottom panels of each figure. The results from the original density matrix for $h \rightarrow e^+ e^- \mu^+ \mu^-$ are taken from [47].

in the first bin, where the negative eigenvalue is comparatively larger. To be conservative, we suppress the low m_{W_2} region in Fig. 5.

For completeness, we also apply this projection method to $h \rightarrow e^+ e^- \mu^+ \mu^-$ channel, where the reconstructed density matrix exhibits significantly larger negative eigenvalues. The results for the original density matrix for $h \rightarrow e^+ \nu_e \mu^- \bar{\nu}_\mu$ are taken from [47]. In Fig. 6 (bottom panel), we show the corresponding concurrence bounds and Frobenius norms. The large differences between the original and projected results for $h \rightarrow e^+ e^- \mu^+ \mu^-$ further underscore that the two-qutrit interpretation of this system is challenged by higher-order corrections.

References

- [1] **ATLAS** Collaboration, G. Aad *et al.*, “Observation of a new particle in the search for the Standard Model Higgs boson with the ATLAS detector at the LHC,” *Phys. Lett. B* **716** (2012) 1–29, [arXiv:1207.7214 \[hep-ex\]](#).

- [2] CMS Collaboration, S. Chatrchyan *et al.*, “Observation of a New Boson at a Mass of 125 GeV with the CMS Experiment at the LHC,” *Phys. Lett. B* **716** (2012) 30–61, [arXiv:1207.7235 \[hep-ex\]](#).
- [3] C. P. Buszello, I. Fleck, P. Marquard, and J. J. van der Bij, “Prospective analysis of spin- and CP-sensitive variables in $H \rightarrow ZZ \rightarrow l(1)+l(1)-l(2)+l(2)-$ at the LHC,” *Eur. Phys. J. C* **32** (2004) 209–219, [arXiv:hep-ph/0212396](#).
- [4] R. M. Godbole, D. J. Miller, and M. M. Muhlleitner, “Aspects of CP violation in the HZZ coupling at the LHC,” *JHEP* **12** (2007) 031, [arXiv:0708.0458 \[hep-ph\]](#).
- [5] S. Bolognesi, Y. Gao, A. V. Gritsan, K. Melnikov, M. Schulze, N. V. Tran, and A. Whitbeck, “On the Spin and Parity of a Single-Produced Resonance at the LHC,” *Phys. Rev. D* **86** (2012) 095031, [arXiv:1208.4018 \[hep-ph\]](#).
- [6] C. Englert, D. Goncalves-Netto, K. Mawatari, and T. Plehn, “Higgs Quantum Numbers in Weak Boson Fusion,” *JHEP* **01** (2013) 148, [arXiv:1212.0843 \[hep-ph\]](#).
- [7] P. Artoisenet *et al.*, “A framework for Higgs characterisation,” *JHEP* **11** (2013) 043, [arXiv:1306.6464 \[hep-ph\]](#).
- [8] F. Caola and K. Melnikov, “Constraining the Higgs boson width with ZZ production at the LHC,” *Phys. Rev. D* **88** (2013) 054024, [arXiv:1307.4935 \[hep-ph\]](#).
- [9] J. M. Campbell, R. K. Ellis, and C. Williams, “Bounding the Higgs Width at the LHC Using Full Analytic Results for $gg \rightarrow e^-e^+\mu^-\mu^+$,” *JHEP* **04** (2014) 060, [arXiv:1311.3589 \[hep-ph\]](#).
- [10] C. Englert and M. Spannowsky, “Limitations and Opportunities of Off-Shell Coupling Measurements,” *Phys. Rev. D* **90** (2014) 053003, [arXiv:1405.0285 \[hep-ph\]](#).
- [11] A. Azatov, C. Grojean, A. Paul, and E. Salvioni, “Taming the off-shell Higgs boson,” *Zh. Eksp. Teor. Fiz.* **147** (2015) 410–425, [arXiv:1406.6338 \[hep-ph\]](#).
- [12] M. Buschmann, D. Goncalves, S. Kuttimalai, M. Schonherr, F. Krauss, and T. Plehn, “Mass Effects in the Higgs-Gluon Coupling: Boosted vs Off-Shell Production,” *JHEP* **02** (2015) 038, [arXiv:1410.5806 \[hep-ph\]](#).
- [13] T. Corbett, O. J. P. Eboli, D. Goncalves, J. Gonzalez-Fraile, T. Plehn, and M. Rauch, “The Higgs Legacy of the LHC Run I,” *JHEP* **08** (2015) 156, [arXiv:1505.05516 \[hep-ph\]](#).
- [14] D. Goncalves, T. Plehn, and J. M. Thompson, “Weak boson fusion at 100 TeV,” *Phys. Rev. D* **95** no. 9, (2017) 095011, [arXiv:1702.05098 \[hep-ph\]](#).
- [15] J. Brehmer, F. Kling, T. Plehn, and T. M. P. Tait, “Better Higgs-CP Tests Through Information Geometry,” *Phys. Rev. D* **97** no. 9, (2018) 095017, [arXiv:1712.02350 \[hep-ph\]](#).
- [16] D. Goncalves, T. Han, and S. Mukhopadhyay, “Off-Shell Higgs Probe of Naturalness,” *Phys. Rev. Lett.* **120** no. 11, (2018) 111801, [arXiv:1710.02149 \[hep-ph\]](#). [Erratum: *Phys.Rev.Lett.* 121, 079902 (2018)].
- [17] CMS Collaboration, A. M. Sirunyan *et al.*, “Measurements of the Higgs boson width and anomalous HVV couplings from on-shell and off-shell production in the four-lepton final state,” *Phys. Rev. D* **99** no. 11, (2019) 112003, [arXiv:1901.00174 \[hep-ex\]](#).
- [18] A. V. Gritsan, J. Roskes, U. Sarica, M. Schulze, M. Xiao, and Y. Zhou, “New features in the

- JHU generator framework: constraining Higgs boson properties from on-shell and off-shell production,” *Phys. Rev. D* **102** no. 5, (2020) 056022, [arXiv:2002.09888 \[hep-ph\]](#).
- [19] D. Gonçalves, T. Han, S. Ching Iris Leung, and H. Qin, “Off-shell Higgs couplings in $H^* \rightarrow ZZ \rightarrow \ell\nu\nu$,” *Phys. Lett. B* **817** (2021) 136329, [arXiv:2012.05272 \[hep-ph\]](#).
- [20] N. C. Hall, I. Criddle, A. Crossland, C. Englert, P. Forbes, R. Hankache, and A. D. Pilkington, “Machine-enhanced CP-asymmetries in the electroweak sector,” *Phys. Rev. D* **107** no. 1, (2023) 016008, [arXiv:2209.05143 \[hep-ph\]](#).
- [21] CMS Collaboration, A. Tumasyan *et al.*, “Measurement of the Higgs boson width and evidence of its off-shell contributions to ZZ production,” *Nature Phys.* **18** no. 11, (2022) 1329–1334, [arXiv:2202.06923 \[hep-ex\]](#).
- [22] ATLAS Collaboration, G. Aad *et al.*, “Evidence of off-shell Higgs boson production from ZZ leptonic decay channels and constraints on its total width with the ATLAS detector,” *Phys. Lett. B* **846** (2023) 138223, [arXiv:2304.01532 \[hep-ex\]](#).
- [23] ATLAS Collaboration, G. Aad *et al.*, “Test of CP-invariance of the Higgs boson in vector-boson fusion production and in its decay into four leptons,” *JHEP* **05** (2024) 105, [arXiv:2304.09612 \[hep-ex\]](#).
- [24] A. Bhardwaj, C. Englert, D. Gonçalves, and A. Navarro, “Nonlinear gauge-Higgs CP violation,” *Phys. Rev. D* **110** no. 11, (2024) 115011, [arXiv:2407.14608 \[hep-ph\]](#).
- [25] A. J. Barr, “Testing Bell inequalities in Higgs boson decays,” *Phys. Lett. B* **825** (2022) 136866, [arXiv:2106.01377 \[hep-ph\]](#).
- [26] J. A. Aguilar-Saavedra, A. Bernal, J. A. Casas, and J. M. Moreno, “Testing entanglement and Bell inequalities in $H \rightarrow ZZ$,” *Phys. Rev. D* **107** no. 1, (2023) 016012, [arXiv:2209.13441 \[hep-ph\]](#).
- [27] R. Ashby-Pickering, A. J. Barr, and A. Wierzychucka, “Quantum state tomography, entanglement detection and Bell violation prospects in weak decays of massive particles,” *JHEP* **05** (2023) 020, [arXiv:2209.13990 \[quant-ph\]](#).
- [28] J. A. Aguilar-Saavedra, “Laboratory-frame tests of quantum entanglement in $H \rightarrow WW$,” *Phys. Rev. D* **107** no. 7, (2023) 076016, [arXiv:2209.14033 \[hep-ph\]](#).
- [29] R. Aoude, E. Madge, F. Maltoni, and L. Mantani, “Probing new physics through entanglement in diboson production,” *JHEP* **12** (2023) 017, [arXiv:2307.09675 \[hep-ph\]](#).
- [30] M. Fabbrichesi, R. Floreanini, E. Gabrielli, and L. Marzola, “Bell inequalities and quantum entanglement in weak gauge boson production at the LHC and future colliders,” *Eur. Phys. J. C* **83** no. 9, (2023) 823, [arXiv:2302.00683 \[hep-ph\]](#).
- [31] M. Fabbrichesi, R. Floreanini, E. Gabrielli, and L. Marzola, “Stringent bounds on HWW and HZZ anomalous couplings with quantum tomography at the LHC,” *JHEP* **09** (2023) 195, [arXiv:2304.02403 \[hep-ph\]](#).
- [32] F. Fabbri, J. Howarth, and T. Maurin, “Isolating semi-leptonic $H \rightarrow WW^*$ decays for Bell inequality tests,” *Eur. Phys. J. C* **84** no. 1, (2024) 20, [arXiv:2307.13783 \[hep-ph\]](#).
- [33] A. Bernal, P. Caban, and J. Rembieliński, “Entanglement and Bell inequalities violation in $H \rightarrow ZZ$ with anomalous coupling,” *Eur. Phys. J. C* **83** no. 11, (2023) 1050, [arXiv:2307.13496 \[hep-ph\]](#).

- [34] R. A. Morales, “Exploring Bell inequalities and quantum entanglement in vector boson scattering,” *Eur. Phys. J. Plus* **138** no. 12, (2023) 1157, [arXiv:2306.17247 \[hep-ph\]](#).
- [35] Q. Bi, Q.-H. Cao, K. Cheng, and H. Zhang, “New observables for testing Bell inequalities in W boson pair production,” *Phys. Rev. D* **109** no. 3, (2024) 036022, [arXiv:2307.14895 \[hep-ph\]](#).
- [36] A. J. Barr, M. Fabbrichesi, R. Floreanini, E. Gabrielli, and L. Marzola, “Quantum entanglement and Bell inequality violation at colliders,” *Prog. Part. Nucl. Phys.* **139** (2024) 104134, [arXiv:2402.07972 \[hep-ph\]](#).
- [37] J. A. Aguilar-Saavedra, “Tripartite entanglement in $H \rightarrow ZZ, WW$ decays,” *Phys. Rev. D* **109** no. 11, (2024) 113004, [arXiv:2403.13942 \[hep-ph\]](#).
- [38] A. Subba and R. Rahaman, “On bipartite and tripartite entanglement at present and future particle colliders,” [arXiv:2404.03292 \[hep-ph\]](#).
- [39] A. Bernal, P. Caban, and J. Rembieliński, “Entanglement and Bell inequality violation in vector diboson systems produced in decays of spin-0 particles,” [arXiv:2405.16525 \[hep-ph\]](#).
- [40] M. Sullivan, “Constraining New Physics with $h \rightarrow VV$ Tomography,” [arXiv:2410.10980 \[hep-ph\]](#).
- [41] J. A. Aguilar-Saavedra, “ $H \rightarrow ZZ$ as a double-slit experiment,” [arXiv:2411.13464 \[hep-ph\]](#).
- [42] M. Grossi, G. Pelliccioli, and A. Vicini, “From angular coefficients to quantum observables: a phenomenological appraisal in di-boson systems,” *JHEP* **12** (2024) 120, [arXiv:2409.16731 \[hep-ph\]](#).
- [43] A. Ruzi, Y. Wu, R. Ding, S. Qian, A. M. Levin, and Q. Li, “Testing Bell inequalities and probing quantum entanglement at a muon collider,” *JHEP* **10** (2024) 211, [arXiv:2408.05429 \[hep-ph\]](#).
- [44] Y. Wu, R. Jiang, A. Ruzi, Y. Ban, X. Yan, and Q. Li, “Testing Bell inequalities and probing quantum entanglement at CEPC,” *Phys. Rev. D* **111** no. 3, (2025) 036008, [arXiv:2410.17025 \[hep-ph\]](#).
- [45] R. Ding, A. Ruzi, S. Qian, A. Levin, Y. Wu, and Q. Li, “Quantum Entanglement between gauge boson pairs at a Muon Collider,” [arXiv:2504.09832 \[hep-ph\]](#).
- [46] M. Del Gratta, F. Fabbri, P. Lamba, F. Maltoni, and D. Pagani, “Quantum properties of $H \rightarrow VV^*$: precise predictions in the SM and sensitivity to new physics,” [arXiv:2504.03841 \[hep-ph\]](#).
- [47] D. Gonçalves, A. Kaladharan, F. Krauss, and A. Navarro, “Quantum Entanglement is Quantum: ZZ Production at the LHC,” [arXiv:2505.12125 \[hep-ph\]](#).
- [48] A. Ruzi, Y. Wu, R. Ding, and Q. Li, “Searching Quantum Entanglement in $p p \rightarrow Z Z$ process,” [arXiv:2506.16077 \[hep-ph\]](#).
- [49] Y. Afik and J. R. M. n. de Nova, “Entanglement and quantum tomography with top quarks at the LHC,” *Eur. Phys. J. Plus* **136** no. 9, (2021) 907, [arXiv:2003.02280 \[quant-ph\]](#).
- [50] M. Fabbrichesi, R. Floreanini, and G. Panizzo, “Testing Bell Inequalities at the LHC with Top-Quark Pairs,” *Phys. Rev. Lett.* **127** no. 16, (2021) 161801, [arXiv:2102.11883 \[hep-ph\]](#).

- [51] C. Severi, C. D. E. Boschi, F. Maltoni, and M. Sioli, “Quantum tops at the LHC: from entanglement to Bell inequalities,” *Eur. Phys. J. C* **82** no. 4, (2022) 285, [arXiv:2110.10112 \[hep-ph\]](#).
- [52] J. A. Aguilar-Saavedra and J. A. Casas, “Improved tests of entanglement and Bell inequalities with LHC tops,” *Eur. Phys. J. C* **82** no. 8, (2022) 666, [arXiv:2205.00542 \[hep-ph\]](#).
- [53] Y. Afik and J. R. M. n. de Nova, “Quantum information with top quarks in QCD,” *Quantum* **6** (2022) 820, [arXiv:2203.05582 \[quant-ph\]](#).
- [54] Y. Afik and J. R. M. n. de Nova, “Quantum Discord and Steering in Top Quarks at the LHC,” *Phys. Rev. Lett.* **130** no. 22, (2023) 221801, [arXiv:2209.03969 \[quant-ph\]](#).
- [55] C. Severi and E. Vryonidou, “Quantum entanglement and top spin correlations in SMEFT at higher orders,” *JHEP* **01** (2023) 148, [arXiv:2210.09330 \[hep-ph\]](#).
- [56] R. Aoude, E. Madge, F. Maltoni, and L. Mantani, “Quantum SMEFT tomography: Top quark pair production at the LHC,” *Phys. Rev. D* **106** no. 5, (2022) 055007, [arXiv:2203.05619 \[hep-ph\]](#).
- [57] Z. Dong, D. Gonçalves, K. Kong, and A. Navarro, “Entanglement and Bell inequalities with boosted $t\bar{t}$,” *Phys. Rev. D* **109** no. 11, (2024) 115023, [arXiv:2305.07075 \[hep-ph\]](#).
- [58] J. A. Aguilar-Saavedra, “Postdecay quantum entanglement in top pair production,” *Phys. Rev. D* **108** no. 7, (2023) 076025, [arXiv:2307.06991 \[hep-ph\]](#).
- [59] T. Han, M. Low, and T. A. Wu, “Quantum Entanglement and Bell Inequality Violation in Semi-Leptonic Top Decays,” [arXiv:2310.17696 \[hep-ph\]](#).
- [60] K. Sakurai and M. Spannowsky, “Three-Body Entanglement in Particle Decays,” *Phys. Rev. Lett.* **132** no. 15, (2024) 151602, [arXiv:2310.01477 \[quant-ph\]](#).
- [61] K. Cheng, T. Han, and M. Low, “Optimizing fictitious states for Bell inequality violation in bipartite qubit systems with applications to the $t\bar{t}$ system,” *Phys. Rev. D* **109** no. 11, (2024) 116005, [arXiv:2311.09166 \[hep-ph\]](#).
- [62] F. Maltoni, C. Severi, S. Tentori, and E. Vryonidou, “Quantum detection of new physics in top-quark pair production at the LHC,” *JHEP* **03** (2024) 099, [arXiv:2401.08751 \[hep-ph\]](#).
- [63] F. Maltoni, C. Severi, S. Tentori, and E. Vryonidou, “Quantum tops at circular lepton colliders,” *JHEP* **09** (2024) 001, [arXiv:2404.08049 \[hep-ph\]](#).
- [64] C. D. White and M. J. White, “Magic states of top quarks,” *Phys. Rev. D* **110** no. 11, (2024) 116016, [arXiv:2406.07321 \[hep-ph\]](#).
- [65] Z. Dong, D. Gonçalves, K. Kong, A. J. Larkoski, and A. Navarro, “Hadronic top quark polarimetry with ParticleNet,” *Phys. Lett. B* **862** (2025) 139314, [arXiv:2407.01663 \[hep-ph\]](#).
- [66] Z. Dong, D. Gonçalves, K. Kong, A. J. Larkoski, and A. Navarro, “Analytical insights on hadronic top quark polarimetry,” *JHEP* **02** (2025) 117, [arXiv:2407.07147 \[hep-ph\]](#).
- [67] K. Cheng, T. Han, and M. Low, “Optimizing entanglement and Bell inequality violation in top antitop events,” *Phys. Rev. D* **111** no. 3, (2025) 033004, [arXiv:2407.01672 \[hep-ph\]](#).
- [68] C. Altomonte, A. J. Barr, M. Eckstein, P. Horodecki, and K. Sakurai, “Prospects for quantum process tomography at high energies,” [arXiv:2412.01892 \[hep-ph\]](#).

- [69] T. Han, M. Low, N. McGinnis, and S. Su, “Measuring Quantum Discord at the LHC,” [arXiv:2412.21158 \[hep-ph\]](#).
- [70] K. Cheng and B. Yan, “Bell Inequality Violation of Light Quarks in Back-to-Back Dihadron Pair Production at Lepton Colliders,” [arXiv:2501.03321 \[hep-ph\]](#).
- [71] Y. Afik *et al.*, “Quantum Information meets High-Energy Physics: Input to the update of the European Strategy for Particle Physics,” [arXiv:2504.00086 \[hep-ph\]](#).
- [72] P. Nason, E. Re, and L. Rottoli, “Spin Correlations in $t\bar{t}$ Production and Decay at the LHC in QCD Perturbation Theory,” [arXiv:2505.00096 \[hep-ph\]](#).
- [73] **ATLAS** Collaboration, G. Aad *et al.*, “Observation of quantum entanglement with top quarks at the ATLAS detector,” *Nature* **633** no. 8030, (2024) 542–547, [arXiv:2311.07288 \[hep-ex\]](#).
- [74] **CMS** Collaboration, “Probing entanglement in top quark production with the CMS detector,” tech. rep., CERN, Geneva, 2024. <https://cds.cern.ch/record/2893854>.
- [75] **CMS Collaboration** Collaboration, “Measurements of polarization and spin correlation and observation of entanglement in top quark pairs using lepton + jets events from proton-proton collisions at $\sqrt{s} = 13$ TeV,” *Phys. Rev. D* **110** (Dec, 2024) 112016. <https://link.aps.org/doi/10.1103/PhysRevD.110.112016>.
- [76] A. Cervera-Lierta, J. I. Latorre, J. Rojo, and L. Rottoli, “Maximal Entanglement in High Energy Physics,” *SciPost Phys.* **3** no. 5, (2017) 036, [arXiv:1703.02989 \[hep-th\]](#).
- [77] S. R. Beane, D. B. Kaplan, N. Klco, and M. J. Savage, “Entanglement Suppression and Emergent Symmetries of Strong Interactions,” *Phys. Rev. Lett.* **122** no. 10, (2019) 102001, [arXiv:1812.03138 \[nucl-th\]](#).
- [78] Q. Liu, I. Low, and T. Mehen, “Minimal entanglement and emergent symmetries in low-energy QCD,” *Phys. Rev. C* **107** no. 2, (2023) 025204, [arXiv:2210.12085 \[quant-ph\]](#).
- [79] M. Carena, I. Low, C. E. M. Wagner, and M.-L. Xiao, “Entanglement suppression, enhanced symmetry, and a standard-model-like Higgs boson,” *Phys. Rev. D* **109** no. 5, (2024) L051901, [arXiv:2307.08112 \[hep-ph\]](#).
- [80] J. Thaler and S. Trifinopoulos, “Flavor patterns of fundamental particles from quantum entanglement?,” *Phys. Rev. D* **111** no. 5, (2025) 056021, [arXiv:2410.23343 \[hep-ph\]](#).
- [81] R. von Kuk, K. Lee, J. K. L. Michel, and Z. Sun, “Towards a Quantum Information Theory of Hadronization: Dihadron Fragmentation and Neutral Polarization in Heavy Baryons,” [arXiv:2503.22607 \[hep-ph\]](#).
- [82] M. Carena, G. Coloretti, W. Liu, M. Littmann, I. Low, and C. E. M. Wagner, “Entanglement Maximization and Mirror Symmetry in Two-Higgs-Doublet Models,” [arXiv:2505.00873 \[hep-ph\]](#).
- [83] J. A. Aguilar-Saavedra, “Quantum tomography beyond the leading order,” [arXiv:2505.11870 \[hep-ph\]](#).
- [84] **ATLAS** Collaboration, G. Aad *et al.*, “Measurement of the angular coefficients in Z -boson events using electron and muon pairs from data taken at $\sqrt{s} = 8$ TeV with the ATLAS detector,” *JHEP* **08** (2016) 159, [arXiv:1606.00689 \[hep-ex\]](#).
- [85] **ATLAS** Collaboration, “Measurement of the effective leptonic weak mixing angle using

- electron and muon pairs from Z -boson decay in the ATLAS experiment at $\sqrt{s} = 8$ TeV,” July, 2018. <https://cds.cern.ch/record/2630340>.
- [86] D. Goncalves and J. Nakamura, “Role of the Z polarization in the $H \rightarrow b\bar{b}$ measurement,” *Phys. Rev. D* **98** no. 9, (2018) 093005, [arXiv:1805.06385](https://arxiv.org/abs/1805.06385) [hep-ph].
- [87] D. Goncalves and J. Nakamura, “Boosting the $H \rightarrow$ invisibles searches with Z boson polarization,” *Phys. Rev. D* **99** no. 5, (2019) 055021, [arXiv:1809.07327](https://arxiv.org/abs/1809.07327) [hep-ph].
- [88] **ATLAS** Collaboration, M. Aaboud *et al.*, “Measurements of top-quark pair spin correlations in the $e\mu$ channel at $\sqrt{s} = 13$ TeV using pp collisions in the ATLAS detector,” *Eur. Phys. J. C* **80** no. 8, (2020) 754, [arXiv:1903.07570](https://arxiv.org/abs/1903.07570) [hep-ex].
- [89] **CMS** Collaboration, A. M. Sirunyan *et al.*, “Measurement of the top quark polarization and $t\bar{t}$ spin correlations using dilepton final states in proton-proton collisions at $\sqrt{s} = 13$ TeV,” *Phys. Rev. D* **100** no. 7, (2019) 072002, [arXiv:1907.03729](https://arxiv.org/abs/1907.03729) [hep-ex].
- [90] R. Mammen Abraham and D. Goncalves, “Boosting new physics searches in $t\bar{t}Z$ and tZj production with angular moments,” *Eur. Phys. J. C* **83** no. 10, (2023) 965, [arXiv:2208.05986](https://arxiv.org/abs/2208.05986) [hep-ph].
- [91] A. Bhardwaj, C. Englert, D. Goncalves, and A. Navarro, “Nonlinear CP violation in the top-Higgs sector,” *Phys. Rev. D* **108** no. 11, (2023) 115006, [arXiv:2308.11722](https://arxiv.org/abs/2308.11722) [hep-ph].
- [92] A. Denner, C. Haitz, and G. Pelliccioli, “NLO EW corrections to polarised $W+W-$ production and decay at the LHC,” *Phys. Lett. B* **850** (2024) 138539, [arXiv:2311.16031](https://arxiv.org/abs/2311.16031) [hep-ph].
- [93] A. Denner, C. Haitz, and G. Pelliccioli, “NLO EW and QCD corrections to polarised same-sign WW scattering at the LHC,” *JHEP* **11** (2024) 115, [arXiv:2409.03620](https://arxiv.org/abs/2409.03620) [hep-ph].
- [94] **CMS** Collaboration, A. Hayrapetyan *et al.*, “Measurement of the Drell–Yan forward-backward asymmetry and of the effective leptonic weak mixing angle in proton-proton collisions at $\sqrt{s} = 13$ TeV,” [arXiv:2408.07622](https://arxiv.org/abs/2408.07622) [hep-ex].
- [95] C. Carrivale *et al.*, “Precise Standard-Model predictions for polarised Z -boson pair production and decay at the LHC,” [arXiv:2505.09686](https://arxiv.org/abs/2505.09686) [hep-ph].
- [96] R. F. Werner, “Quantum states with einstein-podolsky-rosen correlations admitting a hidden-variable model,” *Phys. Rev. A* **40** (Oct, 1989) 4277–4281. <https://link.aps.org/doi/10.1103/PhysRevA.40.4277>.
- [97] P. Rungta, V. Bužek, C. M. Caves, M. Hillery, and G. J. Milburn, “Universal state inversion and concurrence in arbitrary dimensions,” *Phys. Rev. A* **64** (Sep, 2001) 042315. <https://link.aps.org/doi/10.1103/PhysRevA.64.042315>.
- [98] W. K. Wootters, “Entanglement of formation of an arbitrary state of two qubits,” *Phys. Rev. Lett.* **80** (Mar, 1998) 2245–2248. <https://link.aps.org/doi/10.1103/PhysRevLett.80.2245>.
- [99] C. H. Bennett, D. P. DiVincenzo, J. A. Smolin, and W. K. Wootters, “Mixed-state entanglement and quantum error correction,” *Phys. Rev. A* **54** (Nov, 1996) 3824–3851. <https://link.aps.org/doi/10.1103/PhysRevA.54.3824>.
- [100] F. Mintert and A. Buchleitner, “Observable entanglement measure for mixed quantum states,” *Phys. Rev. Lett.* **98** (Apr, 2007) 140505. <https://link.aps.org/doi/10.1103/PhysRevLett.98.140505>.

- [101] C.-J. Zhang, Y.-X. Gong, Y.-S. Zhang, and G.-C. Guo, “Observable estimation of entanglement for arbitrary finite-dimensional mixed states,” *Phys. Rev. A* **78** (Oct, 2008) 042308. <https://link.aps.org/doi/10.1103/PhysRevA.78.042308>.
- [102] ATLAS Collaboration, G. Aad *et al.*, “Combined Measurement of the Higgs Boson Mass from the $H \rightarrow \gamma\gamma$ and $H \rightarrow ZZ^* \rightarrow 4\ell$ Decay Channels with the ATLAS Detector Using $\sqrt{s}=7, 8,$ and 13 TeV pp Collision Data,” *Phys. Rev. Lett.* **131** no. 25, (2023) 251802, [arXiv:2308.04775](https://arxiv.org/abs/2308.04775) [hep-ex].
- [103] M. E. Peskin and D. V. Schroeder, *An Introduction to quantum field theory*. Addison-Wesley, Reading, USA, 1995.
- [104] W. Bernreuther, D. Heisler, and Z.-G. Si, “A set of top quark spin correlation and polarization observables for the LHC: Standard Model predictions and new physics contributions,” *JHEP* **12** (2015) 026, [arXiv:1508.05271](https://arxiv.org/abs/1508.05271) [hep-ph].
- [105] A. Denner, S. Dittmaier, and A. Mück, “PROPHECY4F 3.0: A Monte Carlo program for Higgs-boson decays into four-fermion final states in and beyond the Standard Model,” *Comput. Phys. Commun.* **254** (2020) 107336, [arXiv:1912.02010](https://arxiv.org/abs/1912.02010) [hep-ph].
- [106] A. Denner, S. Dittmaier, M. Roth, and D. Wackerroth, “Predictions for all processes $e^+ e^- \rightarrow 4$ fermions + gamma,” *Nucl. Phys. B* **560** (1999) 33–65, [arXiv:hep-ph/9904472](https://arxiv.org/abs/hep-ph/9904472).
- [107] A. Denner, S. Dittmaier, M. Roth, and L. H. Wieders, “Electroweak corrections to charged-current $e^+ e^- \rightarrow 4$ fermion processes: Technical details and further results,” *Nucl. Phys. B* **724** (2005) 247–294, [arXiv:hep-ph/0505042](https://arxiv.org/abs/hep-ph/0505042). [Erratum: *Nucl.Phys.B* 854, 504–507 (2012)].
- [108] W. S. Cho, K. Choi, Y. G. Kim, and C. B. Park, “M(T2)-assisted on-shell reconstruction of missing momenta and its application to spin measurement at the LHC,” *Phys. Rev. D* **79** (2009) 031701, [arXiv:0810.4853](https://arxiv.org/abs/0810.4853) [hep-ph].
- [109] A. J. Barr and C. G. Lester, “A Review of the Mass Measurement Techniques proposed for the Large Hadron Collider,” *J. Phys. G* **37** (2010) 123001, [arXiv:1004.2732](https://arxiv.org/abs/1004.2732) [hep-ph].
- [110] CMS Collaboration, A. M. Sirunyan *et al.*, “Measurement of the top quark mass in the dileptonic $t\bar{t}$ decay channel using the mass observables $M_{b\ell}$, M_{T2} , and $M_{b\ell\nu}$ in pp collisions at $\sqrt{s} = 8$ TeV,” *Phys. Rev. D* **96** no. 3, (2017) 032002, [arXiv:1704.06142](https://arxiv.org/abs/1704.06142) [hep-ex].
- [111] D. Gonçalves, K. Kong, and J. H. Kim, “Probing the top-Higgs Yukawa CP structure in dileptonic $t\bar{t}h$ with M_2 -assisted reconstruction,” *JHEP* **06** (2018) 079, [arXiv:1804.05874](https://arxiv.org/abs/1804.05874) [hep-ph].
- [112] ATLAS Collaboration, G. Aad *et al.*, “Measurements of Higgs boson production by gluon-gluon fusion and vector-boson fusion using $H \rightarrow WW^* \rightarrow e\nu\mu\nu$ decays in pp collisions at $\sqrt{s} = 13$ TeV with the ATLAS detector,” *Phys. Rev. D* **108** (2023) 032005, [arXiv:2207.00338](https://arxiv.org/abs/2207.00338) [hep-ex].
- [113] CMS Collaboration, A. Tumasyan *et al.*, “Measurements of the Higgs boson production cross section and couplings in the W boson pair decay channel in proton-proton collisions at $\sqrt{s} = 13$ TeV,” *Eur. Phys. J. C* **83** no. 7, (2023) 667, [arXiv:2206.09466](https://arxiv.org/abs/2206.09466) [hep-ex].
- [114] J. Ackerschott, R. K. Barman, D. Gonçalves, T. Heimel, and T. Plehn, “Returning CP-observables to the frames they belong,” *SciPost Phys.* **17** no. 1, (2024) 001, [arXiv:2308.00027](https://arxiv.org/abs/2308.00027) [hep-ph].

- [115] CMS Collaboration, A. Hayrapetyan *et al.*, “Constraints on anomalous Higgs boson couplings from its production and decay using the WW channel in proton–proton collisions at $\sqrt{s} = 13$ TeV,” *Eur. Phys. J. C* **84** no. 8, (2024) 779, [arXiv:2403.00657 \[hep-ex\]](#).
- [116] Z. Dong, K. Kong, K. T. Matchev, and K. Matcheva, “MTN is all you need: Production of multiple semi-invisible resonances at hadron colliders,” *Mod. Phys. Lett. A* **39** no. 31n32, (2024) 2450144, [arXiv:2402.04312 \[hep-ph\]](#).
- [117] ATLAS Collaboration, G. Aad *et al.*, “Measurements of the production cross-sections of a Higgs boson in association with a vector boson and decaying into WW^* with the ATLAS detector at $\sqrt{s} = 13$ TeV,” [arXiv:2503.19420 \[hep-ex\]](#).
- [118] F. Joswig, S. Kuberski, J. T. Kuhlmann, and J. Neuendorf, “pyerrors: A python framework for error analysis of Monte Carlo data,” *Comput. Phys. Commun.* **288** (2023) 108750, [arXiv:2209.14371 \[hep-lat\]](#).
- [119] ALPHA Collaboration, U. Wolff, “Monte Carlo errors with less errors,” *Comput. Phys. Commun.* **156** (2004) 143–153, [arXiv:hep-lat/0306017](#). [Erratum: *Comput.Phys.Commun.* 176, 383 (2007)].
- [120] A. Ramos, “Automatic differentiation for error analysis of Monte Carlo data,” *Comput. Phys. Commun.* **238** (2019) 19–35, [arXiv:1809.01289 \[hep-lat\]](#).
- [121] A. Ramos, “Automatic differentiation for error analysis,” *PoS TOOLS2020* (2021) 045, [arXiv:2012.11183 \[hep-lat\]](#).
- [122] A. Bredenstein, A. Denner, S. Dittmaier, and M. M. Weber, “Precise predictions for the Higgs-boson decay $H \rightarrow WW/ZZ \rightarrow 4$ leptons,” *Phys. Rev. D* **74** (2006) 013004, [arXiv:hep-ph/0604011](#).
- [123] A. Freitas *et al.*, “Theoretical uncertainties for electroweak and Higgs-boson precision measurements at FCC-ee,” [arXiv:1906.05379 \[hep-ph\]](#).
- [124] G. H. Golub and C. F. Van Loan, *Matrix computations (3rd ed.)*. Johns Hopkins University Press, USA, 1996.
- [125] J. R. Johansson, P. D. Nation, and F. Nori, “QuTiP 2: A Python framework for the dynamics of open quantum systems,” *Comput. Phys. Commun.* **184** (2013) 1234–1240, [arXiv:1211.6518 \[quant-ph\]](#).
- [126] J. R. Johansson, P. D. Nation, and F. Nori, “QuTiP: An open-source Python framework for the dynamics of open quantum systems,” *Comput. Phys. Commun.* **183** (2012) 1760–1772, [arXiv:1110.0573 \[quant-ph\]](#).